

Self-assembled nanoporous Pt-based nanowire networks with enhanced oxygen-reduction activity

Henning Galinski,* Thomas Ryll, Yang Lin, Barbara Scherrer, Anna Evans, and Ludwig J. Gauckler
Nonmetallic Inorganic Materials, ETH Zurich, Zurich, Switzerland

Max Döbeli
Ion Beam Physics, ETH Zurich, Zurich, Switzerland

The development of “alternative” power sources poses one of the central scientific challenges of this century. The fuel cell is one of the potential alternatives which can be used for various forms of portable power generation. But in order to stand up to batteries, the fuel cell needs to be safe, reliable and economically competitive.

Even though the implementation of nano-engineered thin-film electrolytes recently caused a leap in evolution of miniaturised fuel cells, the development of a new generation of electrodes has been less effective. This situation is based on the intricate demand to enhance the oxygen-reduction activity while reducing the cost-intensive Pt content of those electrodes. Despite this central challenge, the integrity of those electrodes has to be conserved over a time span of 10000 hours.

Here, we show a solution for both problems, as the nano-porous Pt-based nanowire networks investigated in this contribution guarantee for an enhanced catalytic activity which is up to a factor 13 higher than conventional Pt electrodes. At the same time, we succeeded to reduce the Pt content from 166 $\mu\text{g}/\text{cm}^2$ to 142 $\mu\text{g}/\text{cm}^2$. Furthermore, the analysed nano-porous nanowire networks provide extraordinary thermal stability at elevated temperatures up to 550°C.

I. INTRODUCTION

Platinum is today’s most expensive noble metal. But despite it is enormous costs, Pt has outstanding catalytic properties and is therefore used in numerous modern technologies, ranging from catalytic converters in motor vehicles, chemical reactors and electrochemical devices, such as sensors, batteries and fuel cells [1–3]. Due to its key role in these applications, Pt and its alloys are subject of intense research. One important goal of the

present research efforts is to design new materials that allow for a reduction of the Pt content, i.e. the reduction of the overall costs, without sacrificing the activity, selectivity and stability that Pt guarantees for. A common approach in catalyst design is the so-called d-band engineering [4–6] where experimentally or computationally [7] Pt is alloyed by another catalytic active element, such as Rh, Ru [8], Ni [9, 10], Ir, Y, Pd or Co [2, 11–13]. By doing so, the electronic structure, the d-bands in particular, can be altered and with it the absorption energy of any adsorbing species on the Pt-alloy surface. This is worthwhile as the choice of the alloy material can trigger the selectivity of the Pt-alloy surface in such a way, that only one type of molecules is adsorbed and catalysed. For a more comprehensive and detailed review on the recent progress in the field, especially for fuel cell application, the reader is referred to Ref [1].

In a solid oxide fuel cell, the Pt-alloy catalyst has not only to meet the two requirements described above, but should exhibit long-term stability in hydrogen and oxygen-rich environments at temperatures up to 600°C (873 K). The energy conversion in the cell is achieved by two separated reactions: the hydrogen oxidation reaction (HOR) at the anode and the oxygen reduction reaction (ORR) at the cathode. Thereby, the ORR is typically the rate limiting step of the cell, it involves multiple reaction steps, namely oxygen adsorption, surface diffusion of intermediates, charge transfer and oxygen incorporation into the electrolyte, whose relative speed and spatial arrangement determine the overall reaction mechanism [14]. Insight in the factors that limit the electrode performance is gained by comparing the obtained experimental current-voltage curves to kinetic models that address the electrochemical processes in the fuel cell. These processes cause the chemical conversion of energy in the cell and result in a cell voltage V that is lower than its ideal potential V_0 . For low-temperature fuel cells, the electrode related losses in cell voltage can be described by the Tafel equation [15],

$$V = V_0 - \frac{RT}{\alpha n F} \log \frac{i}{i^*} - i R_{\text{elyt}}. \quad (1)$$

The exchange current density i^* relates to processes at both anode and cathode. R_{elyt} denotes the ohmic drop across the electrolyte, α is the electron transfer coefficient. R, T, n, F have their usual meaning. In order to separate the electrochemical reactions at the anode and cathode, the cell voltage can be expressed by a state-of-

* Current address: Harvard School of Engineering and Applied Sciences, Harvard University, Cambridge, MA 02138, USA; hgalinski@seas.harvard.edu

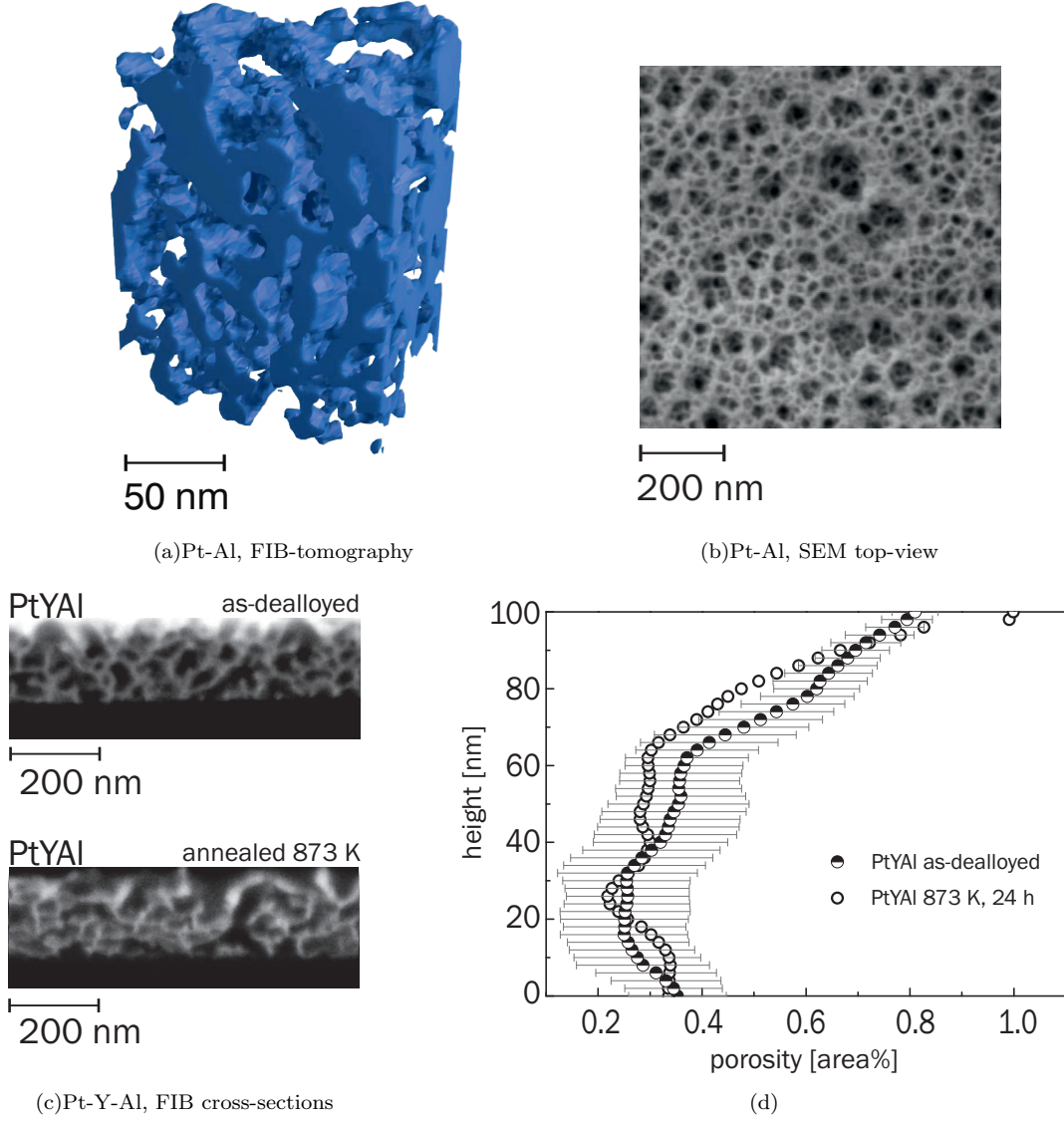


FIG. 1. **Nanowire Networks.** 1(a), Three dimensional (3D) reconstructed FIB thin-film tomography of a $\text{Pt}_{.70}\text{Al}_{.30}$ nanowire network on a YSZ single crystal. The nanowires are interconnected and are characterised by a mean length of 30 nm and a mean diameter of 12 nm. 1(b), Typical scanning electron microscopy top-view image of a nanoporous $\text{Pt}_{.70}\text{Al}_{.30}$ nanowire network. 1(c), FIB-polished cross-sections of a $\text{Pt}_{.60}\text{Y}_{.26}\text{Al}_{.14}$ nanowire network on a YSZ single crystal before and after annealing at 873 K, 24 h. 1(d), Porosity evolution before and after annealing of the $\text{Pt}_{.60}\text{Y}_{.26}\text{Al}_{.14}$ film plotted as a function of the film height perpendicular to the film/substrate interface.

the-art Butler-Volmer model [16], it reads

$$V = V_0 - \left\{ \frac{2}{f} \operatorname{arcsinh} \frac{i}{2i_{\text{anode}}^*} + iR_{\text{elyt}} + \frac{2}{f} \operatorname{arcsinh} \frac{i}{2i_{\text{cathode}}^*} \right\} \quad (2)$$

Thereby f equals F/RT and i_{anode} and i_{cathode} are the electrode specific exchange current densities.

Within this contribution, we propose nanowire networks self-assembled from co-sputtered Pt-Al and Pt-Y-Al thin films as an ideal candidate for high-performance fuel cell electrodes. Briefly, Pt-Al and Pt-Y-Al layers of 300 nm in thickness were deposited at room temperature by

magnetron co-sputtering onto single crystalline yttrium-stabilised zirconia (YSZ) substrates. The assembly of the nanowire networks is achieved by the selective dissolution [17–19] of the less noble constituent (Al) of the Pt-alloy thin film by immersing the coated substrates for up to 60 s in a 4M aqueous solution of NaOH. This process is a simple, fast and cost-effective route to form metal-based nanowire networks of any size.

The selective dissolution of the Al causes a re-assembly of the metal matrix which is characterised by a blood vessel like sponge of connected nanowires with a length

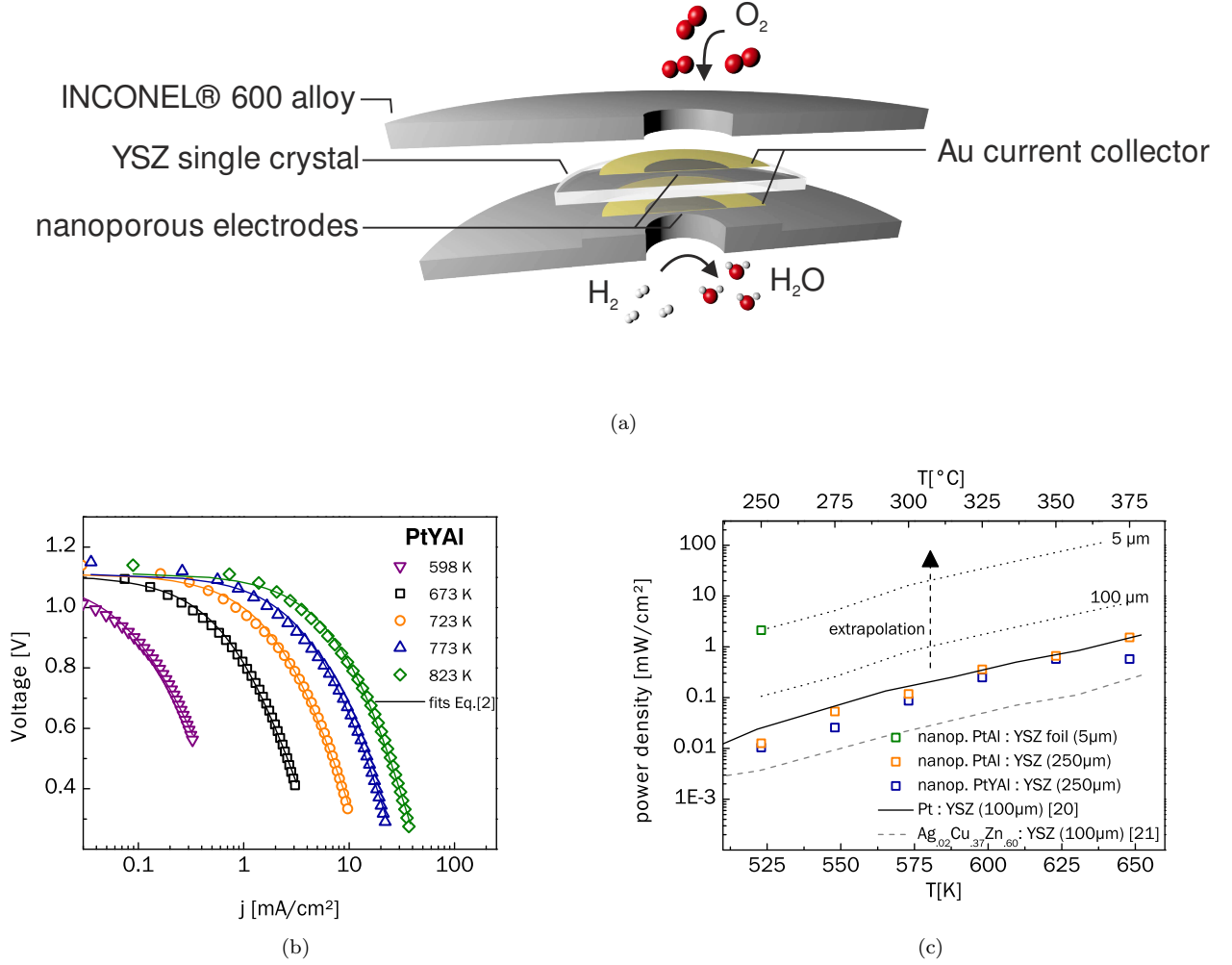


FIG. 2. **Fuel cell setup and device performance.** 2(a), Schematic illustration of the experimental fuel cell setup 2(b). Current-voltage characteristics of the $\text{Pt}_{0.60}\text{Y}_{0.26}\text{Al}_{0.14}$ fuel cells fitted by Eq. 2 (lines) at five different temperatures. 2(c), Measured mean peak power density ρ as function of the operating temperature compared to data from literature [20, 21]. The dotted lines show an extrapolation of the power density (Pt-Al electrodes) for two different electrolyte thicknesses (100 μm , 5 μm). The error bars represent the standard deviation between different cells.

up to 50 nm and typical diameters of ≈ 15 nm. In thin films, this pattern formation is mainly caused by a linearly propagating diffusion front, i.e. the liquid/solid interface, traveling through film at a constant speed [17].

II. RESULTS AND DISCUSSION

In Figure 1(a) and 1(b), the morphology of a dealloyed $\text{Pt}_{0.70}\text{Al}_{0.30}$ nanowire network obtained by thin-film tomography and scanning electron microscopy is shown. The self-assembly of the metal matrix results in a network structure with more than 7000 nanowires per μm^2 . The nanowires have a mean length of 30 nm and a mean diameter of 12 nm. The average in-plane coordination

number $\langle z \rangle$, defined as the average number of touching nanowires per junction in the plane, is $\langle z \rangle = 2.89$.

These electrodes have already a high surface area for fuel absorption and are good electrical conductors but unfortunately undergo both structural and electrochemical degradation that is attributed to the oxidation of residual Al in the nanowires [22]. In order to overcome these problems yttrium has been added as ternary element. This is a promising approach as the addition of yttrium to an alloy is known to increase both, the thermal stability and the resistance to high-temperature oxidation [6]. Moreover, it has been shown by Greeley *et al.*, that the oxygen-reduction activity of bulk Pt_3Y electrodes is up to 10 times higher than the activity of pure Pt [11]. In Fig 1(c) the cross-sectional microstructures of a dealloyed Pt-Y-Al thin film is shown prior and

after annealing at 873 K for 24 hours. Compared to the Pt-Al thin films [22], the addition of yttrium changes the morphology of the nanowire network significantly. These changes manifest in a decrease of the nanowire density to 1500 nanowires per μm^2 , which also decreases the surface area of the electrode. Furthermore, the mean branch diameter increases to 25 nm, alongside with an enhancement of the mean pore intercept length from 10 nm to 35 nm. Despite the decrease in surface area, the addition of yttrium has improved the thermal stability significantly as can already be seen by eye comparing the as-dealloyed and annealed Pt-Y-Al nanowire networks in Fig 1(c). This effect becomes even more evident when the porosity determined by means of multiple cross-sections of as-dealloyed and annealed Pt-Y-Al films is plotted as a function of film height perpendicular to the film/substrate interface (see Fig 1(d)). In contrast to Pt-Al networks, the structural integrity of Pt-Y-Al is conserved after annealing the films at 873 K for 24 hours. The gain in thermal resistance can be attributed to the compositional changes in the nanowire network. Rutherford backscattering spectroscopy showed that the added yttrium replaces the aluminium in the nanowire network and causes a change in composition from $\text{Pt}_{0.70}\text{Al}_{0.30}$ to $\text{Pt}_{0.60}\text{Y}_{0.26}\text{Al}_{0.14}$. As the high surface area is retained, the increased stability and possible enhancement of electrochemical activity should result in a better overall performance in the fuel cell. Despite the residual Al content, the found composition of Pt and Y are in excellent agreement with the nominal composition of the Pt_3Y intermetallic phase of the Pt-Y system [23]. It is noteworthy, that DFT calculations predicted the Pt_3Y alloy to be one of the most stable of all fcc-alloys, where all bonding states are occupied and the anti-bonding states are empty [6].

Fuel cells were constructed using both the Pt-Al and Pt-Y-Al electrodes with an active surface area of 26.6 mm^2 on $250 \mu\text{m}$ thick YSZ single crystal electrolytes. A sketch of the fuel cell design is shown in Fig. 2(a). The cells have been tested with air on the cathode side and a H_2/N_2 mixture on the anode side and operated at temperatures between 523 – 873 K. For each temperature, current-voltage curves of the fuel cell have been measured. A typical set of current-voltage curves as function of temperature for a cell with Pt-Y-Al electrodes is given in Fig. 2(b). The devices are characterised by an open circuit voltage of $V_{\text{OCV}} = 1.08 - 1.15 \text{ V}$ and a maximal power density of $P_{\text{max}} = 4.6 - 5.4 \text{ mW/cm}^2$ at 873 K. The corresponding maximal power density compared to data from literature is shown in Figure 2(c). The power density of our fuel cells falls together with the power densities measured for standard Pt electrodes on $100 \mu\text{m}$ YSZ [20], but it has to be noted that the fuel cell performance is chiefly limited by the electrolyte thickness which is $250 \mu\text{m}$ in this study. Therefore, we conclude that the electrode performance of herein analysed Pt-based nanowire networks is roughly a factor 3 higher than the conventional Pt electrodes [20] and

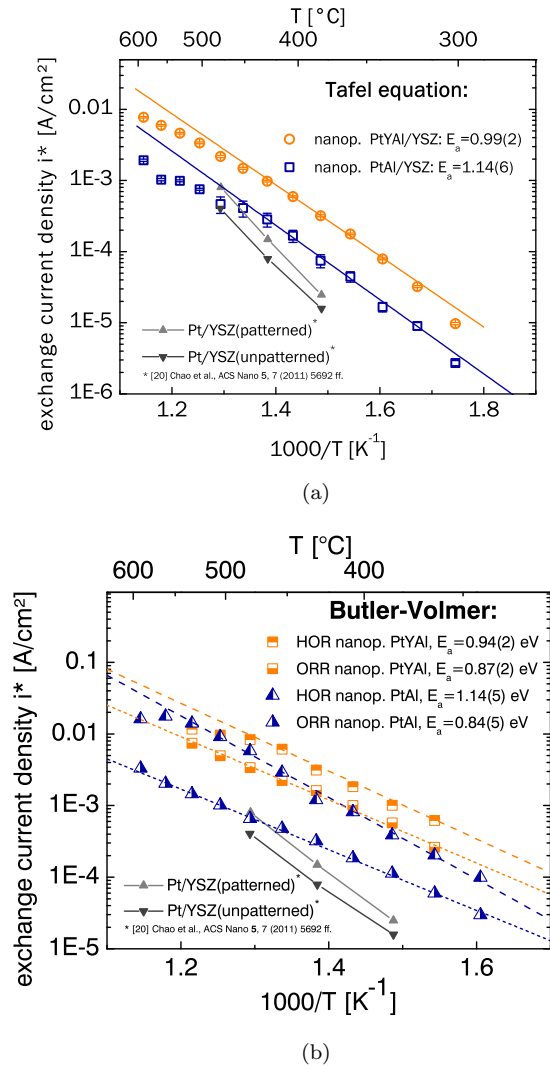


FIG. 3. Exchange current density and thermal activation 3(a) Exchange current density i^* determined by fitting the Tafel equation (Eq.1) to the cells' I-V curves. 3(b) Exchange current density i^* for the ORR and HOR reactions obtained from fits using the Butler-Volmer model (Eq.2).

non-precious electrodes [21]. As proof of concept that the electrolyte thickness is indeed the limiting factor, fuel cells with Pt-Y-Al electrodes and a $5 \mu\text{m}$ thin ceramic YSZ foil [24, 25] as electrolyte have been fabricated as well. Alongside with the to be expected performance of a hypothetical fuel cell with an electrolyte thickness of 5 and $100 \mu\text{m}$ (dotted lines), the result for a fuel cell with a thin YSZ foil as electrolyte and nanoporous Pt-Al electrodes is shown in Fig. 2(c). The found maximal power density of 2.1 mW/cm^2 at 523 K for the Pt-Al electrodes on the YSZ foil is in excellent agreement with the one to be expected.

In order to assess the electrode specific kinetics, the IV curves have been fitted by the Tafel equation (Eq. 1) and the Butler-Volmer model (Eq. 2). The results of

the second are depicted together with the measured I-V curves in Fig. 2(a). Figure 3(a) shows an Arrhenius plot of the estimated exchange current densities i^* obtained for the overall kinetics by the Tafel equation. Compared with conventional Pt electrodes, the exchange current densities for our best nanowire electrodes are a factor 3 (Pt-Al) and 13 (Pt-Y-Al) higher at 648 K than the conventional Pt-electrodes. At higher temperatures, the exchange current density between the conventional electrodes [20] and the Pt-Y-Al electrodes differs by only a factor of 3. Nonetheless, this is still remarkable in terms of reactivity as the Pt content is significantly reduced from $166 \mu\text{g}/\text{cm}^2$ to $142 \mu\text{g}/\text{cm}^2$ while the stability of the electrodes has been increased.

In order to gain more insight on the specific kinetics on the cathode side (ORR) and the anode side (HOR), we used the Butler-Volmer model (Fig. 3(b)). This allows to separate the kinetics at the two electrodes and determine their specific exchange current density $i_{\text{anode,cathode}}^*$. The found HOR for the Pt-Al and the Pt-Y-Al electrode are considerably different not only in the absolute value of the exchange current density but also in the overall thermal activation, that is reduced from $E_{\text{a,Pt-Al}} = 1.14 \text{ eV}$ to $E_{\text{a,Pt-Y-Al}} = 0.94 \text{ eV}$ as consequence of the yttrium addition. On the cathode side, solely the absolute value of the exchange current density, thus the oxygen reactivity is positively affected. This considerable enhancement in ORR and HOR activity can be attributed to the reduced oxygen adsorption energy and hydrogen adsorption energy on Pt_3Y in respect to pure Pt [11]. The enhanced activity can be understood in terms of the d-band model, as the addition of the early transition metal yttrium lowers the d-band centre with respect to the Fermi level, which decreases the binding energy between the catalyst and O_2 or H_2 respectively and therefore the overpotential of the ORR and HOR. Obviously, this results in a considerable boost in fuel cell performance.

III. CONCLUSION

Self-assembled nanoporous electrodes are an exciting and promising candidate for fuel cells and other electrochemical devices. They are characterised by a interconnected high surface area and a high thermal stability. They are versatile, as their catalytic properties and morphologies can be designed via alloying up to some extent. And as the pattern formation is achieved via self-assembly and not by typical top-bottom processes, large areas can be nano-structured in a cost-effective way. Moreover these nanowire networks show exceptional catalytic activity that outperform conventionally designed catalysts by up to a factor of 13. In case of the analysed Pt_3Y electrodes, we were able to show that besides the catalytic activity even the thermal stability is enhanced considerably. These electrodes withstand temperatures

higher than 823 K and as they were fabricated by etching in 4M NaOH, they should even be stable under highly acidic conditions. The found scaling of both the catalytic and thermal properties of the Pt and Pt_3Y nanowire electrodes are in excellent agreement with findings for bulk-catalysts of the same type [11]. In particular, the results show that the catalytic properties of these nanowire networks can be tailored by d-band engineering. Further studies examining the catalytic activity of nanowire networks with a mean branch diameter below 15 nm should shed new light on the role of geometrical confinement on the catalytic properties at the nanoscale.

IV. EXPERIMENTAL METHODS

A. Thin Film Preparation and Characterisation

Pt-Al and Pt-Y-Al layers of 300 nm in thickness, were deposited at room temperature by magnetron co-sputtering ($P_{\text{Pt}} = 37 \text{ W}$, $P_{\text{Al}} = 252 \text{ W}$, $p_{\text{Ar}} = 2 \cdot 10^{-3} \text{ mbar}$) and ($P_{\text{Pt}} = 28 \text{ W}$, $P_{\text{Y}} = 32 \text{ W}$, $P_{\text{Al}} = 252 \text{ W}$, $p_{\text{Ar}} = 2 \cdot 10^{-3} \text{ mbar}$) onto single crystalline yttrium-stabilised zirconia substrates that were pre-cleaned using isopropanol and acetone.

The substrates coated with the Pt-Al and Pt-Y-Al thin films were etched in 4M NaOH at room temperature in a time domain between 20 – 60 s and rinsed in deionised water afterwards. The morphological analysis of the samples was studied via scanning electron microscopy (SEM) assisted by focused ion beam etching (FIB). Single and multiple cross-sections of the dealloyed both, the Pt-Al and the Pt-Y-Al system were cut, polished and imaged using a Zeiss NVISION 40 FIB etching system. The stacks of multiple cross-sections were aligned recursively by Stackreg [26] and reconstructed using AVS Express (Advanced Visual Systems Inc.) and Blender (The Blender Foundation). The voxel-size of the resulting tomographic images is not cubic and $1 \times 1 \times 3 \text{ nm}^3$ in size. The morphological parameters such as the nanowire density and the average coordination number $\langle z \rangle$ have been determined using MATHEMATICA's morphology package. The compositional analysis was performed by Rutherford backscattering spectroscopy (RBS) experiments using a 2MeV ^4He beam and a standard silicon surface barrier detector at 165° . Since the thermal stability of the nanowire networks at elevated temperatures is a critical issue for a successful application in a fuel cell, the Pt-Y-Al films were subjected to successive heating in a muffle furnace at 873 K for 24 h in air and were analysed by SEM and FIB afterwards.

B. Fuel Cell Setup and Electrochemical Characterisation

Pt-Al and Pt-Y-Al nanowire networks were fabricated symmetrically on both sides of 250 μm thick YSZ single

crystals. In order to prove the performance dependence on the electrolyte thickness Pt-Al electrodes were fabricated on 5 μm thin YSZ foils as well. A detailed description of the preparation of these ceramic foils for fuel cell devices is given elsewhere [24, 25]. The fuel cell devices have been electrochemically characterised by Electrochemical Impedance Spectroscopy (EIS). Electrochemical impedance spectra and IV curves were acquired with an IM6 workstation (Zahner Elektrik, Germany) at the open-circuit voltage (OCV). Uniform and reproducible contacting was assured by deposition of 500-nm thick Au frames overlapping the Pt-based electrodes (see also Fig. 2(a)). The Au frames were sputtered during 4 min with 60 mA at 50 bar and a target-substrate distance of 6 cm in a SCD 050 sputter coater (Bal-tec, Liechtenstein). Flattened Pt wires were screwed onto the INCONEL®600 fuel cell holder. Temperature was controlled by a tube furnace constantly flushed with 300 sccm air on the cathode side and a mixture of 240 sccm N_2 and 60 sccm H_2 at anode side. The ohmic drop across the electrolyte iR_{elyt} has been subtracted before fitting the I-V curves with Eq. 1 and 2 and was used for the extrapolation.

V. ACKNOWLEDGEMENTS

T.R. and H.G. designed the experiment, Y.L. performed the experiment and conducted the FIB imaging, T.R. and B.S. deposited the thin films, A.E. fabricated the thin ceramic YSZ foils, M.D. performed the Rutherford backscattering spectroscopy experiments, L.G. gave scientific support, conceptual advice and edited the manuscript. H.G. wrote the main manuscript, analysed the experimental data and conducted the FIB imaging. All authors discussed the results and implications and commented on the manuscript at all stages. H. Galinski gratefully acknowledges financial support from the *Size Matters!*-project, Switzerland. The authors would like to thank the EMEZ (Electron Microscopy Center, ETH Zurich) and the FIRST clean-room team for their support. H.G. thanks P. Gasser for outstanding FIB maintenance and I. Schenker for peripatetic discussions. The authors declare that they have no competing financial interests.

-
- [1] Debe, M. K. Electrocatalyst approaches and challenges for automotive fuel cells. *Nature* **486**, 43–51 (2012).
 - [2] Stamenkovic, V. *et al.* Trends in electrocatalysis on extended and nanoscale Pt-bimetallic alloy surfaces. *Nature Materials* **6**, 241–247 (2007).
 - [3] Steele, B. C. H. & Heinzel, A. Materials for fuel-cell technologies. *Nature* **414**, 345–352 (2001).
 - [4] Greeley, J., Nørskov, J. K. & Mavrikakis, M. Electronic structure and catalysis on metal surfaces. *Annual Review of Physical Chemistry* **53**, 319–348 (2002). PMID: 11972011.
 - [5] Viswanathan, V., Hansen, H. A., Rossmeisl, J. & Nørskov, J. K. Universality in oxygen reduction electrocatalysis on metal surfaces. *ACS Catalysis* **2**, 1654–1660 (2012).
 - [6] Jóhannesson, G. H. *et al.* Combined electronic structure and evolutionary search approach to materials design. *Phys. Rev. Lett.* **88**, 255506 (2002).
 - [7] Nørskov, J., Bligaard, T., Rossmeisl, J. & Christensen, C. Towards the computational design of solid catalyst. *Nature Chemistry* **1**, 37–46 (2009).
 - [8] Jiang, X., Gür, T. M., Prinz, F. B. & Bent, S. F. Atomic layer deposition (ald) co-deposited Pt-Ru binary and Pt skin catalysts for concentrated methanol oxidation. *Chem. Mater.* **22**, 3024–3032 (2010).
 - [9] Stamenkovic, V. *et al.* Improved oxygen reduction activity on $\text{Pt}_3\text{Ni}(111)$ via increased surface site availability. *Science* **315**, 493–497 (2007).
 - [10] Snyder, J., Livi, K. & Erlebacher, J. Oxygen reduction reaction performance of [mtbd][beti]-encapsulated nanoporous NiPt alloy nanoparticles. *Advanced Functional Materials* **23**, 5494–5501 (2013).
 - [11] Greeley, J. *et al.* Alloys of platinum and early transition metals as oxygen reduction electrocatalysts. *Nat Chem* **1**, 552–556 (2009).
 - [12] Oezaslan, M., F., H. & Strasser, P. Pt-based core-shell catalyst architectures for oxygen fuel cell electrodes. *Journal of Physical Chemistry Letters* **4**, 3273–3291 (2013).
 - [13] Snyder, J., Fujita, T., Chen, M. & Erlebacher, J. Oxygen reduction in nanoporous metal-ionic liquid composite electrocatalysts. *Nature Materials* **9**, 904–907 (2010).
 - [14] Nørskov, J. K. *et al.* Origin of the overpotential for oxygen reduction at a fuel-cell cathode. *The Journal of Physical Chemistry B* **108**, 17886–17892 (2004).
 - [15] Wolf Vielstich, H. A. G., Arnold Lamm (ed.) *Handbook of Fuel Cells: Fundamentals, Technology, Applications* (WILEY, 2003).
 - [16] Biesheuvel, P. M., Francoc, A. A. & Bazant, M. Z. Diffuse charge effects in fuel cell membranes. *J. Electrochem. Soc.* **156**, B225–B233 (2009).
 - [17] Galinski, H. *et al.* Dealloying of platinum-aluminum thin films: Dynamics of pattern formation. *Phys. Rev. Lett.* **107**, 225503 (2011).
 - [18] Erlebacher, J., Aziz, M. J., Karma, A., Dimitrov, N. & Sieradzki, K. Evolution of nanoporosity in dealloying. *Nature* **410**, 450–453 (2001).
 - [19] Erlebacher, J. & Sieradzki, K. Pattern formation during dealloying. *Scripta Materialia* **49**, 991 – 996 (2003).
 - [20] Chao, C.-C. *et al.* Enhanced oxygen exchange on surface-engineered yttria-stabilized zirconia. *ACS Nano* **7**, 2186–2191 (2013).
 - [21] Holme, T. P. & Prinz, F. B. Nonprecious metal catalysts for low temperature solid oxide fuel cells. *J. Phys. Chem.*

- 115**, 11641–11648 (2011).
- [22] Ryll, T. *et al.* Dealloying of platinum-aluminum thin films: Electrode performance. *Phys. Rev. B* **84**, 184111 (2011).
 - [23] Palenzona, A. & Cirafici, S. The Pt-Y (platinum-yttrium) system. *Bulletin of Alloy Phase Diagrams* **11**, 493–497 (1990).
 - [24] Bonderer, L. J., Chen, P. W., Kocher, P. & Gauckler, L. J. Free-standing ultrathin ceramic foils. *Journal of the American Ceramic Society* **93**, 3624–3631 (2010).
 - [25] Evans, A., Bieberle-Hütter, A., Bonderer, L. J., Stuckenholz, S. & Gauckler, L. J. Micro-solid oxide fuel cells using free-standing 3 mol. % yttria-stabilised-tetragonal-zirconia-polycrystal electrolyte foils. *Journal of Power Sources* **196**, 10069 – 10073 (2011).
 - [26] Thévenaz, P., Ruttimann, U. & Unser, M. A pyramid approach to subpixel registration based on intensity. *IEEE Transactions on Image Processing* **7**, 27–41 (1998).